DEVELOPMENT OF A FORCE RESULTANT MODEL FOR SPUDCANS ON DENSE SANDS BASED ON CENTRIFUGE STUDIES

N. Cheng* and M. J. Cassidy
Centre for Offshore Foundation Systems
UNIVERSITY OF WESTERN AUSTRALIA

** corresponding author: ning.cheng@research.uwa.edu.au*

ABSTRACT

Jack-up drilling rigs are usually supported by multiple large inverted cone shape foundations with a sharp protruding spigot, i.e., the so-called spudcan. In the present study, a strain-hardening plasticity based force resultant model was developed to predict the load-displacement behaviour of a spudcan under combined vertical (V), horizontal (H) and moment (M) loads. This model was developed from the observation of a series of specifically designed centrifuge experiments. A recently developed *VHM* apparatus was used in this study with an upgraded mechanical system to incorporate high stress testing conditions. The primary merit of the apparatus is the allowance of independent vertical, horizontal and rotational movements of the footing. As such, this study is considered to be the first comprehensive centrifuge study for investigating spudcan behaviour under all *VHM* loading directions on dense frictional material. A total of 16 individual tests were performed at an acceleration of 100 times that of the Earth's gravity. The results indicate that the yield surface previously derived from 1-*g* laboratory tests on loose sand is conservative for dense sand under properly scaled stress condition. Retrospective simulation of the experimental tests verifies the model's suitability in the stability assessment of jack-up units subjected to combined loading. The spudcan's behaviour is also compared to previous studies of flat circular obtained at 1-*g* with the aim of describing the changes of the behaviours.

KEY WORDS: bearing capacity, centrifuge modeling, force-resultant models

INTRODUCTION

Jack-up rigs are mobile drilling facilities used frequently within the oil and gas industry. Jack-ups are increasingly being used in harsher environments for longer periods, resulting in a need for accurate assessment of jack-up capacity under extreme storm conditions. The structural capability of a jack-up is crucially dependent upon the unit's foundation fixity. Being able to predict the spudcan's behaviour under combined loads will provide insight into the jack-up capacities and sensitivities and hence prevent or minimise the consequences of unexpected 'incidents'.

Traditionally, in the site assessment of jack-up platforms, the footings have been modelled as pinned, (i.e. full vertical and horizontal restraint and zero rotational fixity). The reason is a belief that this produces conservative results, though this has been shown to not always be the case (see [30] for details). A slightly more complex assumption has been to assume simple linear springs (e.g. [23]). However, spudcan-soil interaction has been shown to be nonlinear that simple springs cannot model. Extensive study has been

undertaken to determine a more appropriate model of the foundation behaviour. Included in these studies is the plasticity based strain-hardening approach that directly predicts the behaviour of a spudcan in the soil in terms of the applied force combination and corresponding displacements. The principal concept is that at any penetration of a foundation into the soil, a yield surface will be established. The shape of this yield surface is assumed to be constant, but its size may vary as a function of footing penetration depth. Within the yield surface, the deformation is assumed as elastic, but load points touching the yield surface will cause plastic deformation. Therefore, the key components included in a single surface strain-hardening plasticity model are the following: (i) an empirically determined yield surface defining the boundary between elastic and plastic responses, (ii) a set of elastic constants to define any incremental changes of load within the yield surface, (iii) a hardening law to specify the relationship between the size of the yield surface and the plastic vertical deformation, and (iv) a flow rule that determines the ratio between the plastic strains. Previous studies in the context of plasticity models are predominately based on small-scale 1-g experiments [27; 17; 18; 7; 22; 2]; however, even with the use of a centrifuge, only limited load paths were investigated, mostly on loose to medium sand [32; 8; 20; 21; 12; 13]. This predominance of such small-scale 1-g experiments occurred because only a fixed arm, or at best, a hinged arm could be used in the centrifuge tests. The same limitations also applies to recent studies of the footing's behaviour on dense sand [3; 15]. Because centrifuge experiments are of limited load combinations more comprehensive centrifuge evidence of behaviour at stress levels relevant offshore will build confidence in the use of these models in engineering practice.

This paper addresses this with the interpretation of results from a comprehensive programme investigating spudcan behaviours on dense sand for all *VHM* load directions and conducted at an acceleration of 100 times that of Earth's gravity in the drum centrifuge at the University of Western Australia (UWA). The main aim of the experiments was to develop a plasticity based force resultant model for characterisation a spudcan footing's behaviour on dense sand under combined loadings. This study follows similar experiments on loose sand [13]. Comparisons of behaviour between loose sand with the dense sand results of this study are made.

EXPERIMENTAL SETUP

The centrifuge located at UWA is rated to 400-g with a diameter of 1.2 m [29]. A soil sample is contained in an annular channel of 0.2 m in radial depth and 0.3 m in height. Tests were performed at an acceleration of 100 times that of Earth's gravity (referred to as 100-g).

All tests conducted in this study were displacement–controlled. Loading was applied to a load reference point (LRP) at the centreline of the foundation at the mud line level. The sign convention for the loads and displacements and the LRP adopted here follow the standardised convention system proposed by [5] for combined loadings. The load was described by horizontal translation (u), vertical translation (w) and rotation (θ) ; the positive sign conventions together with the footing size dimensions are shown in Fig. 1.

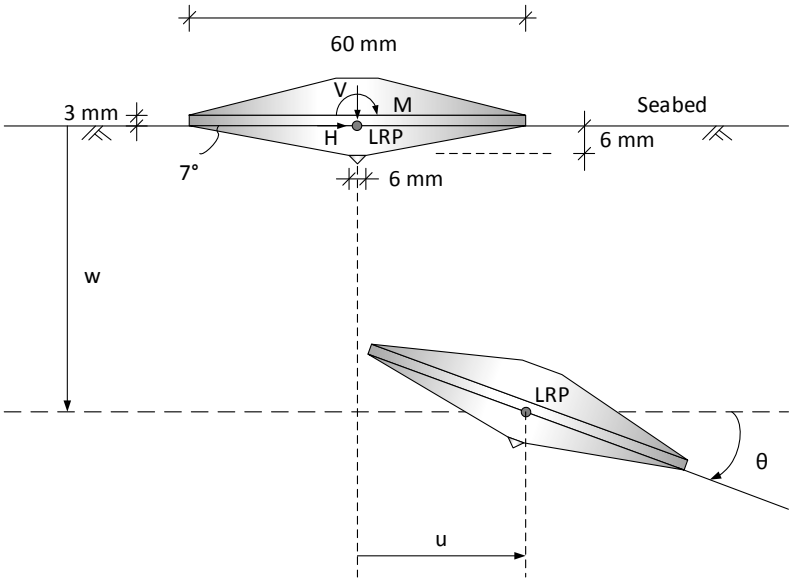

Fig. 1 Model dimensions and sign conventions for the load and displacements

A specialised *VHM* apparatus that allows independent vertical, horizontal and rotational movements of the footing was used in this study. This apparatus consists of two horizontal actuators and one vertical actuator connected through aluminium made mechanical components, such as hinges and linkage arms. The entire apparatus was mounted to the tool table so it can be subjected to vertical movements. Any demands involving rotation will require all three actuators to move simultaneously in a controlled speed so that the footing connected at the end could rotate in a small angle ($\leq 13°$) around the LRP. This series of movements are calculated according to the external demand by a build-in-house program established using the NI LabVIEW platform [25]. More details of the apparatus can be found in [33] and [14], and use of this apparatus for *VHM* loading in loose sand is discussed in [12; 13]. A schematic of the loading arm connected with the *VHM* actuator is presented in Fig. 2.

(a) (b)

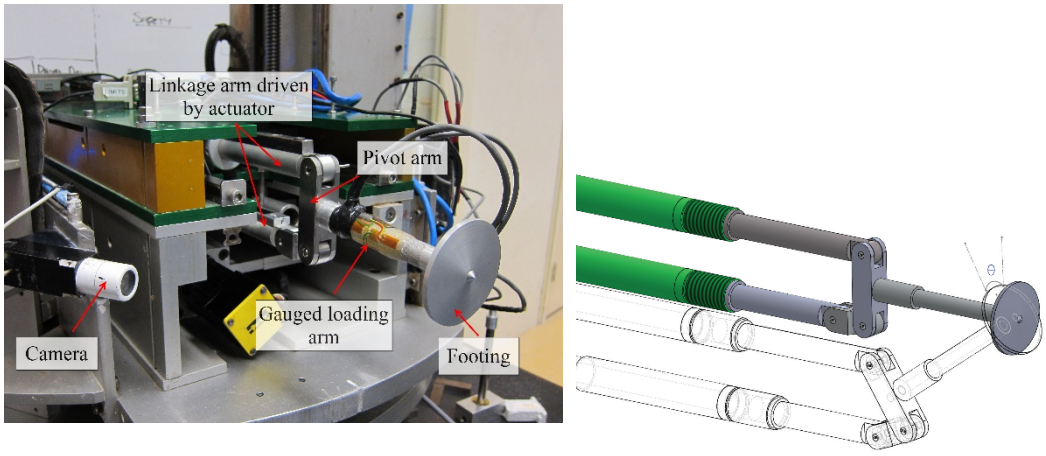

Fig. 2 Schematic of the *VHM* loading arm

The sand sample was prepared by using a retrofitted rotating actuator mounted to the tool table. UWA silica sand ($e_{min} = 0.49$, $e_{max} = 0.76$, $D_{50} = 0.20$, $e_{max} = 0.76$, and $D_{50} = 0.20$ mm) was poured into the rotating outer channel of the drum centrifuge via a hose at 20-g (Fig. 3). The distance between the hose outlet to the sample surface was maintained to a constant value through a wireless controlled actuator. While the height of sand in the channel increased, the actuator was driven back by a corresponding distance. The sand surface was levelled before water was introduced from the base of the channel. The sample height was 140 mm and 20 mm of water remained on top of the sample throughout the testing. A consistent relative density of ≈90% was interpreted using 8 cone-penetrometer tests performed in-flight, as shown in Fig. 4. The interpretation of the cone penetrometer tests follows the procedure established by [28]. A comparison to the average relative density derived from the same number of cone-penetrometer tests on the loose sample of [13] is also shown in Fig. 4.

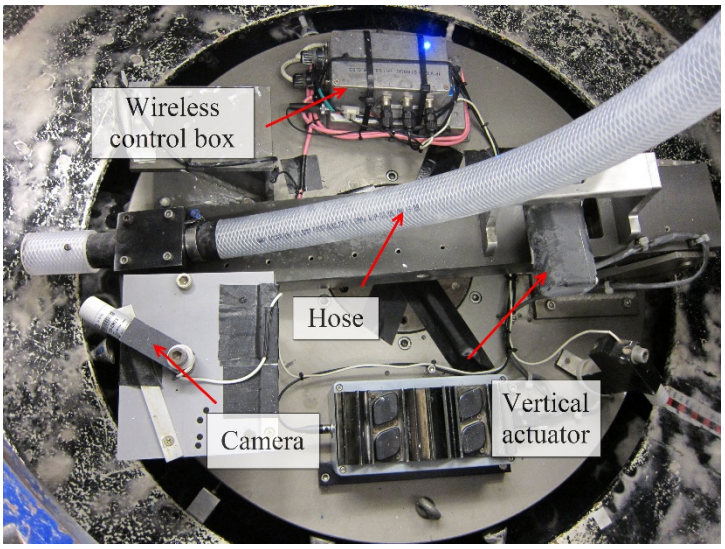

Fig. 3 Rotating actuator for the sand sample preparation

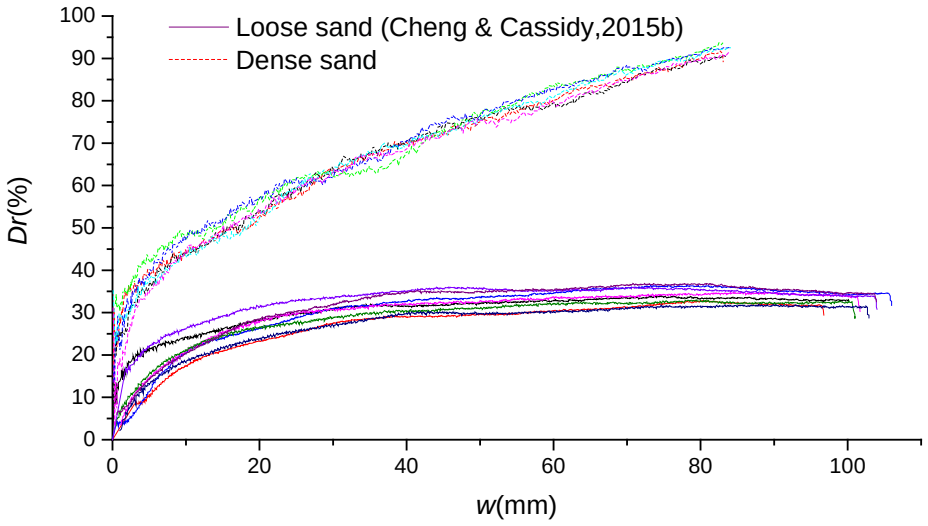

Fig. 4 Cone-penetrometer tests results

EXPERIMENTAL PLAN

Four individual groups of tests were performed in this study, with each of them targeting one particular component of the plasticity model. Particular attention was given to the calibration of the yield surface and the flow rule parameters required for establishment of the force resultant models. The tests conducted are as follows:

a) One vertical penetration test to establish the vertical load-displacement benchmarks,
b) One vertical load-unload loop to provide an estimate of the vertical elastic stiffness,
c) Seven swipe tests to investigate the yield surface at specific stress levels,
d) Seven radial displacement tests to investigate the flow rule.

Further details of the experimental plan are listed below:

TABLE 1: Details of the performed experimental plan

Test type	Test name	V (N)	V / A (kPa)	$u / 2R\theta$	w (mm)	u (mm)	θ (radians)
Vertical penetration	S_D_VP1	4371	1546	-	7.4	-	-
Load-unload loops	S_D_VP2	5112	1808	-	7.0	-	-
Swipe tests	S_D_SW1	1206	427	∞	3.0	9	0
	S_D_SW2	1632	577	0.952	3.6	6	0.105
	S_D_SW3	1503	532	0.190	3.5	1.2	0.105
	S_D_SW4	2124	751	-0.286	3.9	-1.8	0.105
	S_D_SW5	2051	725	-0.571	3.7	-3.6	0.105
	S_D_SW6	2064	730	-1.143	3.8	-7.2	0.105
	S_D_SW7	1998	707	-1.724	3.8	-6	0.058
Radial displacement tests	S_D_RD1	3278	1159	-	5	5	-
	S_D_RD2	3284	1161	-	5	2.5	-
	S_D_RD3	3115	1102	-	5	7.5	-
	S_D_RD4	3278	1159	-	5	-	0.087
	S_D_RD5	3492	1235	-	5	-	0.026
	S_D_RD6	3269	1156	-	5	-	0.131
	S_D_RD7	3455	1222	-	5	-	0.044

V represent values at the beginning of the swipe; A : the footing area; $2R$: footing diameter

RESULTS AND DISCUSSION

First introduced by Tan (1990) and extensively used by [19] and [24], the swipe test is an effective method for directly exploring the yield surface. The results of selected representative swipe tests will be discussed first, followed by the radial displacement tests. The results from the vertical penetration test will be described in the section of the force resultant model development.

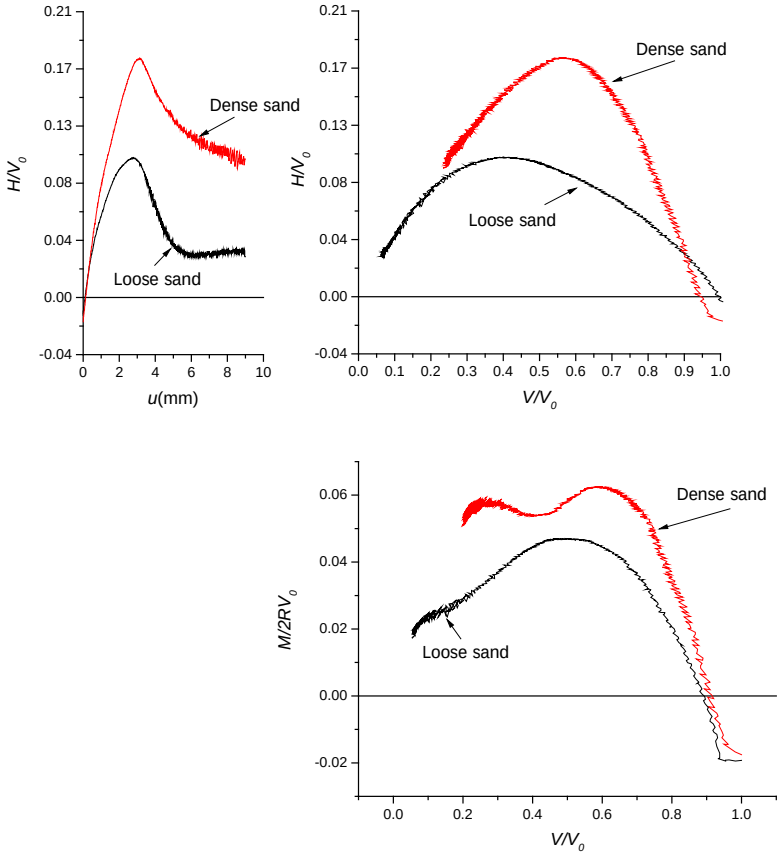

Fig. 5 Swipe test S_D_W1 compared with loose sand results of equivalent swipe (u/2Rθ = ∞)

Fig. 5 shows the normalised swipe results for test S_D_SW1 with $u/2R\theta = \infty$ (the loads measured are normalised by the vertical load achieved before the swipe, known as V_0). The load path and load-displacement response recorded during the test were projected onto the *VH* plane and compared with the same test that was performed on loose sand (swipe from $V/A \approx 450$ kPa, $u/2R\theta = \infty$,see [12]). A significant change in both the shape and the size of the yield surface is observed. In addition, the load paths on loose sand exhibit a more ductile behaviour post-peak. This result implies the yield surface previously derived from loose sand is conservative for dense sand at high stress.

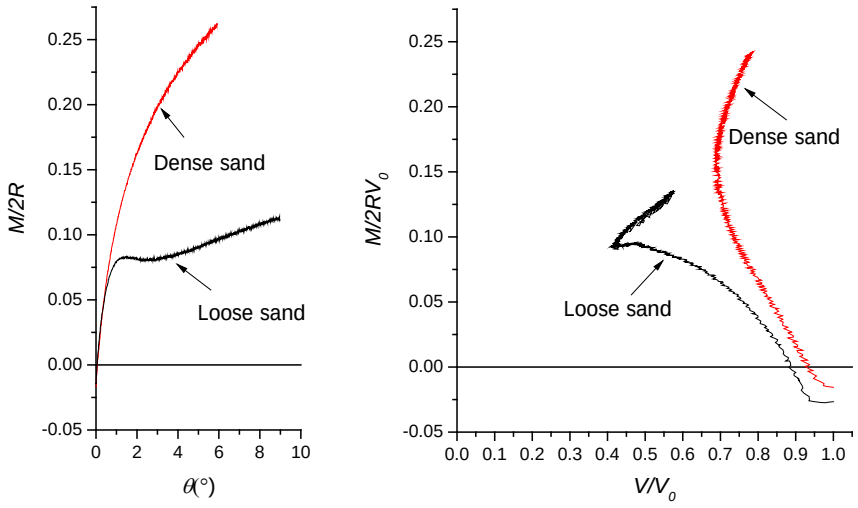

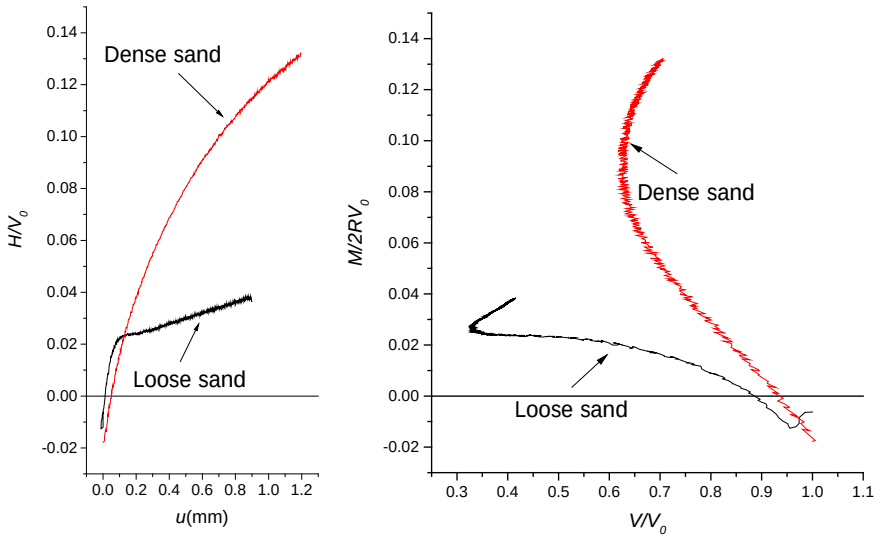

Fig. 6 Swipe test S_D_SW4 compared with the loose sand results

Fig. 6 presents the same comparison for swipe test S_D_SW4 with $u / 2R\theta = -0.095$. A straight frictional sliding line was observed in the tail section of the load path, similar to what was observed on loose sand (see [12]). The dissimilarity is that there is no transition point in the dense sand test that clearly differentiates the load path traced along the yield path and the subsequent frictional sliding line. Strong dilatant behaviour is observed in all tests as the footing load increases just prior to the load path joining the sliding line.

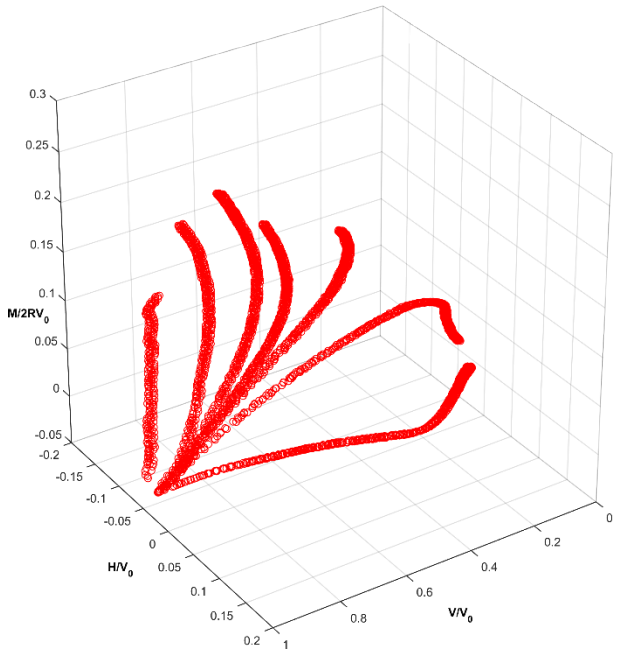

Fig. 7 Swipe load paths in normalised three-dimensional space

Fig. 7 presents all the swipe load paths grouped in normalised three-dimensional space. Frictional sliding lines were widely observed in all swipe tests involving a high moment ratio a similar behaviour also observed at 1-g in dense sand tests conducted by [6]. Further observation shows that those frictional sliding

lines all lie on one surface, which means a three-dimensional sliding surface may also exist for the dense sand condition similar to what observed in [12].

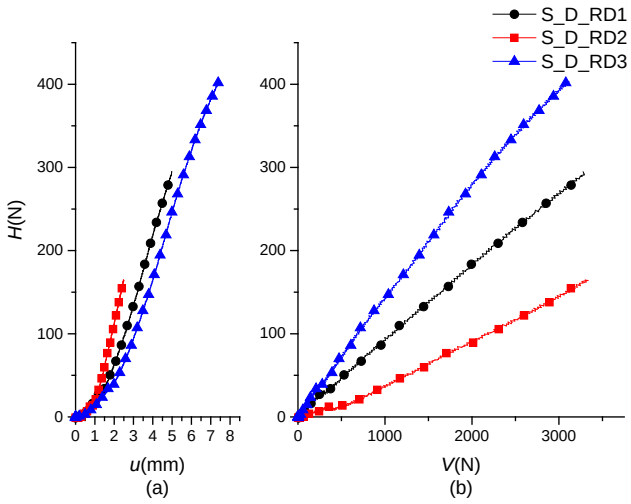

Fig. 8 Radial displacement test with combined horizontal and vertical loadings

Grouped in Fig. 8 are the results for the radial displacement tests S_D_RD1, S_D_RD2 and S_D_RD3. The pattern of the behaviour is very similar to straight lines; as the ratio $\delta u / \delta w$ increases, so does the slope of the load path H / V .

DEVELOPMENT OF THE FORCE RESULTANT MODEL

An existing strain-hardening plasticity model for circular footing on dense sand silica sand forms the basis of the present work. This model, as described by [22] and [9], is also known as Model C was initially developed for flat circular footings. In the present study, modification is necessary for Model C to be suitable for modelling the spudcan foundation on dense sand subjected to combined loads. This modification includes a recalibrated hardening law expression, yield surface, flow rule and an additional sliding surface that intersects the yield surface observed in this study.

HARDENING LAW

The strain-hardening expression, known as the hardening law, defines the variation of the size of the yield surface. For most shallow foundation models, the size of the yield surface is a function of the plastic component of the vertical displacement [19; 9]. When the footing is pushed into the soil, the shape of the yield surface is assumed to be constant; however, its size expands with the amount of plastic vertical displacement (w_p). Fig. 9 indicates consistency in the vertical loading response of the two vertical loading tests S_D_VP1 and S_D_VP2. From the figure, an average elastic stiffness can be established as 2.7 kN/mm.

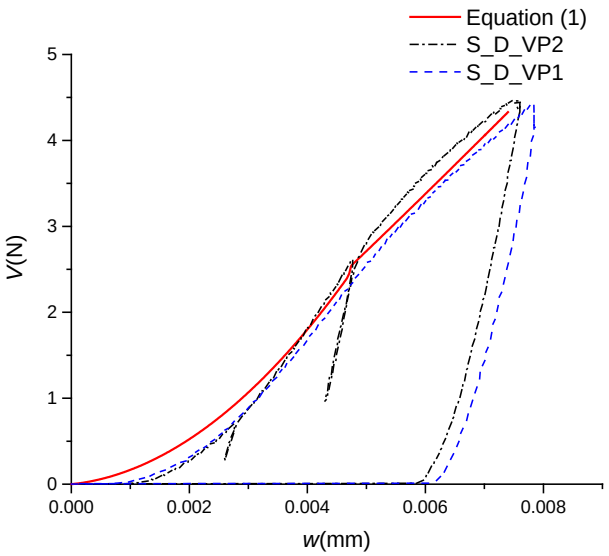

Fig. 9 Vertical penetration test

A vertical load penetration curve is obtained simply by performing a pure vertical loading test (for pure vertical loading, $V_0 = V$) and adjusting for the plasticity in the soil. Because previous hardening laws that were derived from small scale model experiments at 1-g have not been proven regarding their relevance for large footing under high stress, an empirical strain-hardening expression that fits the silicon sand experimental data [21] was calibrated against experimental data in this study. The functional form is

$$V_0 = cw_p \frac{1 + w_p / k_1}{1 + w_p / k_2} \qquad (1),$$

where w_p was divided into two parts to account for the cone shape underside: for $w_p < 0.003$ m, the best fit dimensionless parameters are found to be $c = 151.9$, $k_1 = 0.000704$, and $k_2 = 109.7$; and for $w_p > 0.003$ m, the best parameters are $c = 855.8$, $k_1 = 156.1$, and $k_2 = 0.04$. Equation (1) is plotted in Fig. 9 in terms of the total vertical displacement.

ELASTIC STIFFNESS

To identify the parameters required to describe the elastic behaviour within the yield surface, several vertical load-unload loops were performed. With the yield surface established, elastic behaviour is expected (as long as the loading (or displacement) increment is fully contained within this yield surface) and was defined using the finite element methods of [1], [26] and [16]. Research indicates that cross coupling does exists between the horizontal and rotational footing displacements [1]. As recommended by [22], the elastic relationship between the increments of load (dV, dM, dH) and the corresponding elastic displacements (dw, $d\theta$, du) for a flat circular footing is:

$$\begin{Bmatrix} dV \\ dM/2R \\ dH \end{Bmatrix} = 2GR \begin{bmatrix} k_V & 0 & 0 \\ 0 & k_M & k_C \\ 0 & k_C & k_H \end{bmatrix} \begin{Bmatrix} dw \\ 2Rd\theta \\ du \end{Bmatrix} \quad (2),$$

where G is a representative elastic shear modulus, and k_V, k_M, k_H, k_C are dimensionless elastic constants for the elastic behaviour within the yield surface. The appropriate values for circular foundations, as listed in [1], are:

k_V = 2.65; k_M = 0.46; k_H = 2.30; k_C = -0.14.

The shear modulus G was estimated by the following formula (recommended by [22]):

$$\frac{G}{p_a} = g\sqrt{\frac{V}{Ap_a}} \quad (3),$$

where p_a is atmospheric pressure, V is a representative vertical load on the foundation, A is the plan area of the foundation and g is a dimensionless constant. In the current study, an average G is calculated with the above-mentioned elastic stiffness, k_V, as 15.5 N/mm^2, which compares well with the data from [2] of 12.7 N/mm^2. With the shear modulus available, it is then possible to subtract the elastic vertical displacement calculated from the measured total displacement for each data point to obtain plastic displacements. When the derivation of the elastic stiffness k_V is not available from load-unload loops, a typical value of g suggested by [11] is approximately 400 for practical offshore conditions.

YIELD SURFACE

The yield surface is a boundary that separates the elastic and plastic states in *VHM* space. The determination of the yield surface from experiments is a crucial part of the development of the plasticity model. A key assumption in the strain-hardening plasticity theory is that the shape of the yield surface remains constant, but its size is directly related to the plastic vertical penetration depth. Displacement-controlled swipe tests were used to explore the yield surface shape, in which the footing was initially penetrated to the desired depth before being subject to combined horizontal and rotational displacements, while the vertical displacement was held constant. The combined load path recorded in the swipe event is believed to replicate the yield surface very closely at that embedment. Note that the experimental data were corrected for rig and soil elasticity, following the procedure suggested by [19].

The chosen three-dimensional surface that fits the observed behaviour of footings well is that originally proposed by [24] from their experimental swipe tests in a 1-*g* environment. This equation has been widely used to describe the behaviour of footings on various sands, such as in [7], [9] and [2], and was also used to fit the yield surface of spudcans in loose sand by [12]; [13]. This surface is defined as

$$f=\left(\frac{H}{h_0V_0}\right)^2+\left(\frac{M/2\mathrm{R}}{m_0V_0}\right)^2-\frac{2\alpha HM/2R}{h_0m_0V_0^{\,2}}-\left[\frac{(\beta_1+\beta_2)^{(\beta_1+\beta_2)}}{\beta_1^{\beta_1}\beta_2^{\beta_2}}\right]^2\left(\frac{V}{V_0}\right)^{2\beta_1}\left(1-\frac{V}{V_0}\right)^{2\beta_2}=0 \qquad (4),$$

in which, V_0 is the apex of the surface and determined by the hardening law. h_0 and m_0 determine the yield surface in the horizontal and moment directions, respectively. Shape factor α accounts for the rotation of the elliptical cross section in the $M/2R:H$ plane. β_1 and β_2, as introduced following [27], are the shape parameters for the yield surface in the vertical load plane. In this study, the best fit parameters are found to be $h_0=0.174$, $m_0=0.143$, $\alpha=-0.042$, $\beta_1=0.98$ and $\beta_2=0.99$. Fig. 10 shows a great consistency when comparing the measured experimental data with the proposed yield surface normalised in the $M/2R:H$ plane. Note that the apex appearing at approximately $V/V_0=0.9$ is attributed to the swipes that began with a small amount of negative bending moment developed along the vertical penetration prior to the swipe event.

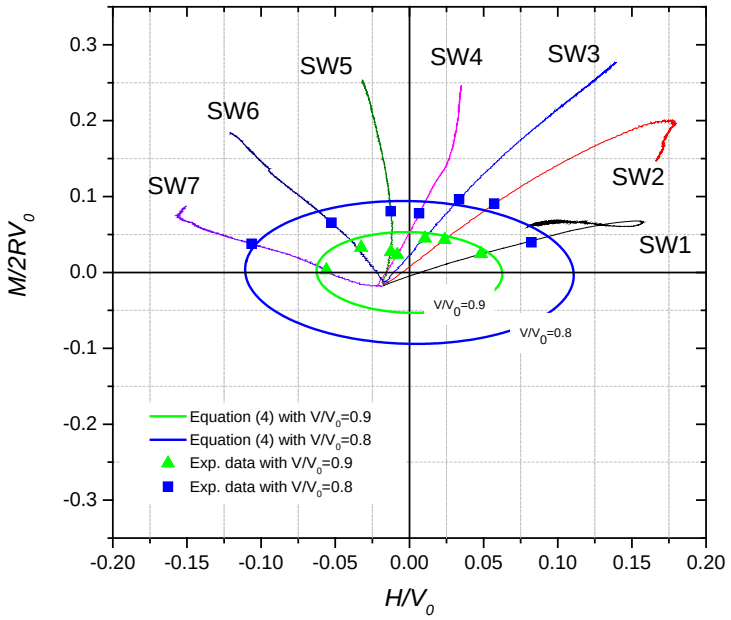

Fig. 10 Comparison between the analytical *VHM* yield surface and the experimental data for the swipe tests

The quality of the fitting can be visually confirmed by introducing the quantity Q as

$$Q=\sqrt{\left(\frac{H}{h_0}\right)^2+\left(\frac{M/2R}{m_0}\right)^2-\frac{2\alpha HM/2R}{h_0m_0}} \qquad (5).$$

Fig. 11 shows the load paths of all swipe tests being projected onto the VQ plane. The experimental results show a fair comparison with the quantity described by Equation (5), validating the best-fit parameters described above.

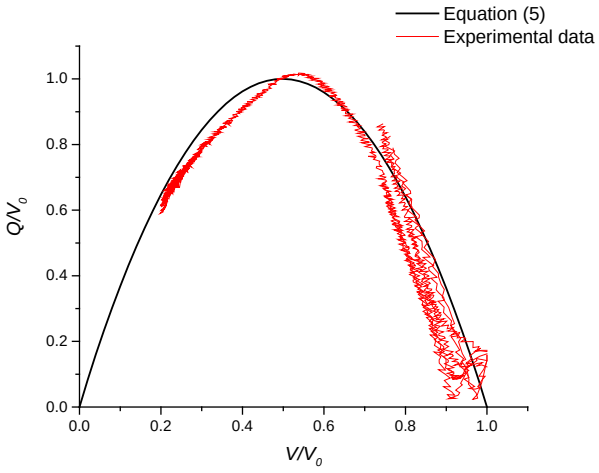

Fig. 11 Swipe load paths on the normalised *VQ* plane

SLIDING SURFACE

Similar to previous tests conducted on loose sand (see [12]), observation of a sliding surface implies that the shearing failure occurred under the footing. This failure mechanism is believed to be closely related to horizontal and moment resistance under combined loading conditions and also to the mobilised sand internal friction angle ϕ. This additional intersecting surface for spudcans in loose sands was described in the form of

$$q\left(\frac{V}{V_0},\frac{H}{V_0},\frac{M/2R}{V_0}\right)=\frac{1}{\tan\phi}\left(\frac{H}{V_0}\right)-4\left(\frac{M/2R}{V_0}\right)+\frac{V}{V_0}=0 \qquad (6),$$

by assuming a simple Coulomb failure criterion. It was derived by assuming a triangular distribution of stress under the footing (see [12]) and the mobilised sand internal friction angle ϕ estimated to be $34.3°$. However, in this study, Equation (6) was found not to provide the best fit. This lack of agreement is because in dense sand the assumption of triangular stress distribution is not appropriate; thus, a more realistic parabola shaped stress distribution (see [4]) should be applied (Fig. 12), meaning a higher moment resistant is expected.

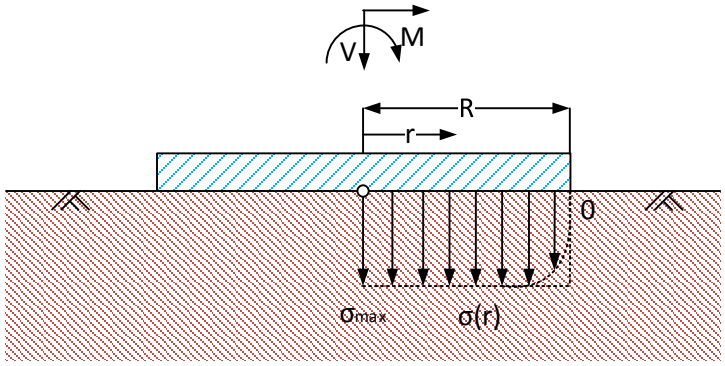

Fig. 12 Assumed stress distribution for a circular footing on dense sand

Again, if a simple Coulomb failure criterion for pure shearing is assumed, then a parabola shaped stress distribution underneath the footing can be approximated as rectangular shape; thus,

$$\tau(r)=\sigma(r)\tan\phi \qquad (7),$$

where ϕ is the internal friction angle of the sand, $\sigma(r)$ is the vertical stress defined with the assumed stress distribution in Equation (4) and $\tau(r)$ is the shear stress. Similarly, if the footing is subjected to pure vertical and moment loadings under drained condition (Fig. 12), then it can be assumed that, only half of the area underneath the footing is in contact with the soil. Therefore, by integrating the stresses over the entire area, the total vertical load is

$$V = \int_0^R \sigma(r)(\pi r)dr = \frac{1}{2}\pi R^2 \sigma_{\max} \quad (8),$$

and the corresponding total moment load is

$$M = \int_0^R \sigma(r)(\pi r)\,\mathrm{r}\,dr = \frac{1}{3}\pi R^3 \sigma_{\max} \quad (9).$$

Combining the vertical and moment capacities together result in

$$\frac{M/2R}{V} = \frac{1}{3} \quad (10),$$

substituting Equation (10) into Equation (6), we have the general analytical form of the sliding surface for dense sand as:

$$q\left(\frac{V}{V_0}, \frac{H}{V_0}, \frac{M/2R}{V_0}\right) = \frac{\mu}{\tan\phi}\left(\frac{H}{V_0}\right) - \varpi\left(\frac{M/2R}{V_0}\right) + \frac{V}{V_0} = 0 \quad (11),$$

where, $\mu = 1$ and $\varpi = 3$. Therefore, the gradient of the slope of the moment component of this additional sliding surface is higher for loose (factor of 4 in Equation 6) than dense sand (factor of 3 in Equation 11), reflecting a more even distribution of stress under the footing. Both equations fit the data exceptionally well, as already shown for loose sands by [12] and as shown below and in Figures 13 to 15 for the dense sand data of this study.

The determination of the internal friction angle ϕ mobilised in the centrifuge is not so straightforward and requires an iterative solution. The approach to approximately quantify the value of ϕ was established by [31] because the peak friction angle is equal to the critical-state friction angle, ϕ_{crit}, plus an additional component that depends on the relative dilatancy:

$$\phi = \phi_{crit} + mI_R \quad (12),$$

where the constant m was taken as 3 for the triaxial or general stress, and I_R is the relative dilatancy defined by [4] as a function of the relative density I_D, the strength parameter Q, and the mean stress level p' as follows:

$$I_R = I_D\left(Q - \ln p'\right) - 1 \quad (13),$$

The mean stress p' can be expressed as

$$p' = \lambda q_{nom} \quad (14),$$

where q_{nom} is the nominal bearing pressure (evaluated from the bearing pressure from the start of the swipe tests), and λ is a representative stress factor. Alternatively, De Beer (1967) also presented the following expression for p':

$$p' = \left(\frac{1}{1+\tan^2\phi}\right)\left(\frac{1}{1+\sin\phi}\right)\frac{q_{nom}+3\gamma' d}{4} \quad (15),$$

where γ' and d are the effective unit weight and the footing diameter, respectively. Using Q=10 and ϕ_{crit} =31° (a typical value for UWA superfine silicon sand), an iterative scheme was adopted here in determining a suitable ϕ that satisfy Equations (11) and (14) simultaneously. In this study, ϕ was estimated to be 44.3°. With ϕ defined, the theoretical sliding surface is determined. Fig. 13 demonstrates the proposed yield surface of Equation (4) incorporated with the theoretical sliding surface of Equation (11) in normalised three-dimensional space. The load paths that are divergent from the yield surface all clearly lie on this particular sliding surface.

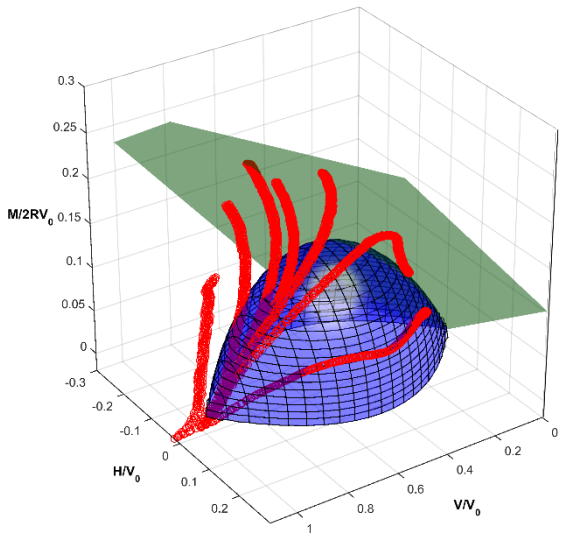

Fig. 13 Yield surface incorporated sliding surface in normalised three-dimensional space

To better evaluate the fit, the proposed yield surface along with the sliding surface was sliced cut with the $M/2RH$ ratio taken from the experiments and then projected to the VH and VM planes (so that two dimensional plots can be made). Two examples are shown in Fig. 14 and Fig. 15, which also demonstrate the comparison between the model prediction and the experimental data of two typical swipe events: S_D_SW1 with high horizontal load component ($u/2R\theta = \infty$) and S_D_SW3 with high moment load component ($u/2R\theta = 0.095$). Both predictions are in excellent agreement with the experimental observations.

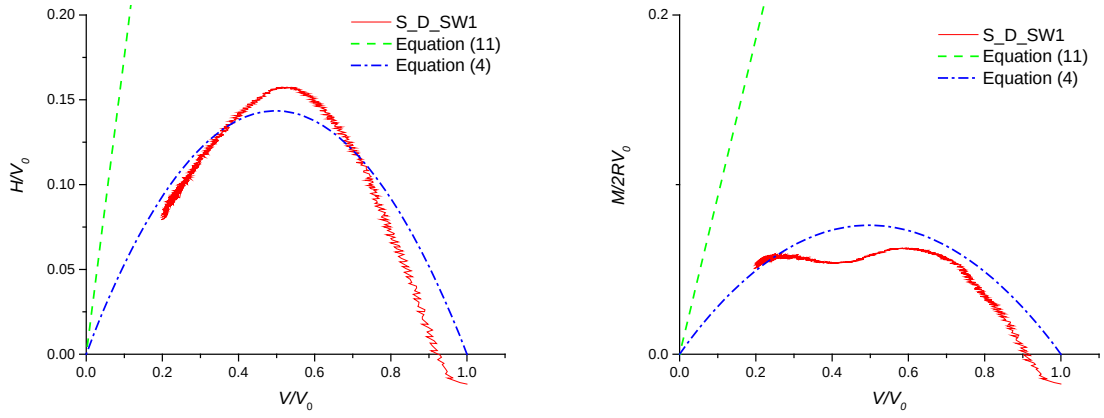

Fig. 14 Comparison between the model prediction and experimental data S_D_SW1

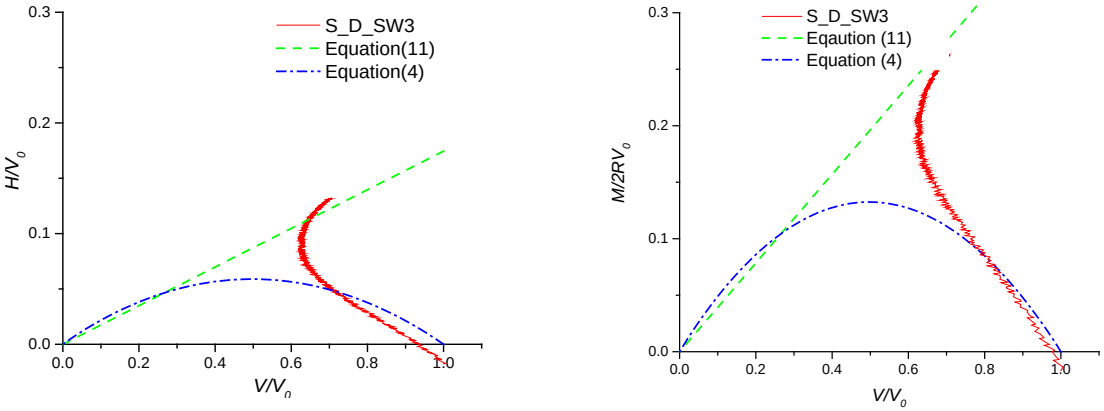

Fig. 15 Comparison between the model prediction and experimental data S_D_SW3

INTERPRETATION OF THE HORIZONTAL AND MOMENT BEARING CAPACITIES

Accurately predicting the size of the yield surface under various relative densities is of importance to geotechnical engineers. [3] and [15] both reported in their studies that the yield surface observed on dense sand is significantly larger than that of loose sand. However, with only limited load paths investigated in their studies, such a conclusion cannot be drawn with confidence. The experimental evidence obtained in present study addresses this limitation.

The simplest way to quantify the effect on the size of the yield surface is by comparing $h_{0dense} / h_{0loose} \approx m_{0dense} / \mathrm{m}_{0loose} \approx 1.5$ directly. This comparison provides a direct indication of the change of the size. [3] also reported that $q_{0dense} / q_{0loose} \approx 1.8$ for the torsional capacity of flat footing in centrifuge tests, which is slightly higher than the findings from the current study.

Alternatively, [6] provided relevant evidence that the stress level may affect the shape of the normalised yield surface in their 1-g tests on dense sand. They proposed that the size of the yield surface changes in relation to the ratio of the vertical load (V) and the vertical peak bearing capacity (V_{peak}).

This relationship is defined as

$$h_0 = h_{0\,peak}\left[1 - 0.36\ln\left(\frac{V_0}{V_{peak}}\right)\right] \quad (16),$$

and

$$m_0 = m_{0\,peak}\left[1 - 0.36\ln\left(\frac{V_0}{V_{peak}}\right)\right] \quad (17).$$

For the spudcan shape, V_{peak} can be approximated using the classical bearing capacity theory as

$$V_{peak} = N_\gamma \gamma' \pi R^3 \quad (18).$$

where N_γ can be obtained from the [10], and ϕ obtained using the previously discussed interactive approach. This hypothesis was validated against data obtained in this study. [6] recommended using $h_{0\,peak} = 0.11$ and $m_{0\,peak} = 0.08$, hence, a constant h_0 can be used for all V_0. Fig. 16 shows the measured horizontal and moment capacities in current study with the theoretical predictions from Equation (16) and (17) and h_0 and m_0 values from previous studies. As shown in Fig. 16, the results of this study are slightly lower than the 1-g studies described by [6]. This is in line with the findings of [15]. However, more swipe tests under various stress levels are still required before this conclusion can be safely confirmed.

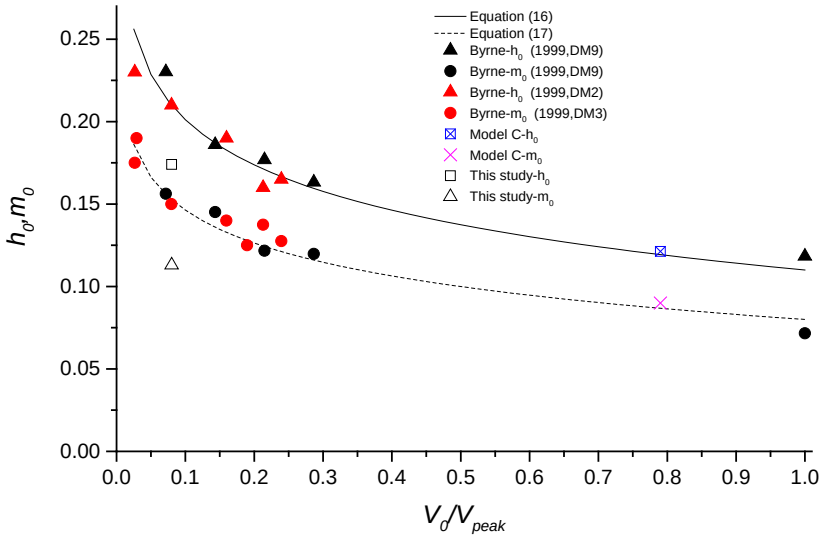

Fig. 16 Comparison of the measured horizontal and moment capacities with the theoretical predictions from Equation (16) and (17)

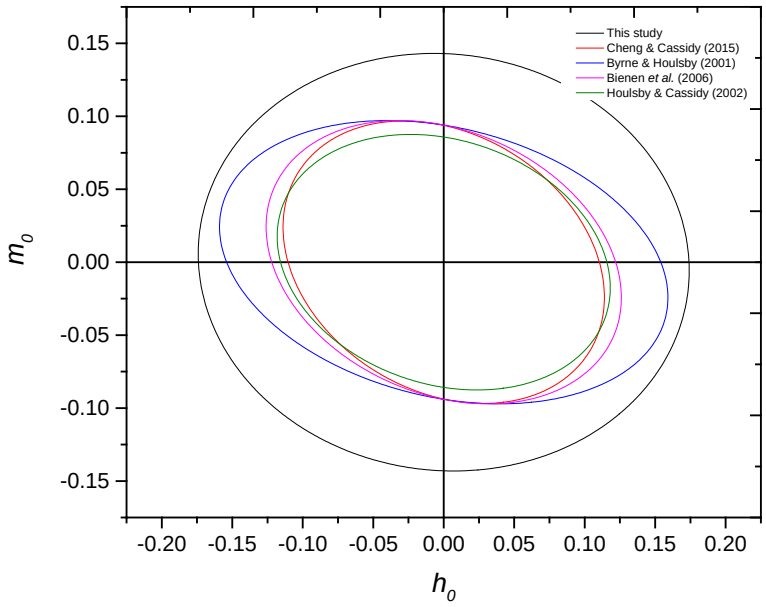

Fig. 17 Comparison of the horizontal and moment bearing capacities

Fig. 17 compares the yield surface obtained in the current study with previously available results from 1-*g* tests on loose sand. Clearly, at the high stress levels in the centrifuge, the yield surface was observed to be much larger than previously observed in small scale 1-*g* tests and on loose sand. The eccentricity of the dense sand model in the current study is also found to be different from those of previous studies.

FLOW RULE

A flow rule is used to determine the ratio between plastic displacement components when a load state reaches the yield surface result during further plastic penetration and expansion of the yield surface. Further analysis of the data indicate that the associated assumption in *VH* and *VM* planes is not valid. In the current study, the plastic potential is formulated as

$$g=\left(\frac{H}{\alpha_h h_0 V_0'}\right)^2+\left(\frac{M/2R}{\alpha_m m_0 V_0'}\right)^2-\frac{2\alpha HM/2R}{\alpha_h\alpha_m h_0 m_0 V_0'}-\beta_{34}{}^2\left(\frac{V}{V_0'}\right)^{2\beta_3}\left(1-\frac{V}{V_0'}\right)^{2\beta_4}=0 \qquad (19)$$

where

$$\beta_{34}=\frac{(\beta_3+\beta_4)^{(\beta_3+\beta_4)}}{\beta_3{}^{\beta_3}\beta_4{}^{\beta_4}}$$

where α_h and α_m are non-dimensional horizontal and moment 'association' factors, respectively, and V_0' is a dummy parameter denoting the intersection of the plastic potential with the *V* -axis. The parameters β_3 and β_4 are chosen to allow for different variations in the curvature. If $\alpha_h,\alpha_m=1$ and $\beta_3=\beta_4=1$, then the plastic potential coincides with the yield surface, and associated flow is implied. As the experimental data did not support the associated flow assumption, it can be further derived that

$$\frac{\delta q_p}{\delta w_p} = \frac{\partial f / \partial Q}{\partial f / \partial V} \tag{20},$$

where δq_p is the generalised plastic displacement conjugate to Q ,which ca be expressed as

$$\delta q_p = \sqrt{\frac{1}{1-e^2}[(\mathrm{h}_0\, \delta u_\mathrm{p})^2 + (\mathrm{m}_0\, 2R\delta\theta_p)^2 + 2e(\mathrm{h}_0\, \delta u_\mathrm{p})(\mathrm{m}_0\, 2R\delta\theta_p)]} \tag{21}.$$

Therefore $\delta q_p / \delta w_p$ can be determined, numerically adjusting the $\alpha_h, \alpha_m, \beta_3, \beta_4$ values so that the difference between the calculated $\delta q_p / \delta w_p$ values and experimental measured $\delta q_p / \delta w_p$ values is minimum. With the plastic potential defined by Equation (20), the following values were deemed to provide the best fit $\alpha_h = 3.3$, $\alpha_m = 6.1$, $\beta_3 = 0.01$, $\beta_4 = 0.68$. The associated flow, measured experimental data (represented by solid dots) and predictions from non-associated flow (represented by hollow dots) is shown in Fig. 18. It is clear that the associated flow does no describe the experimental data satisfactorily, but the predictions with the above-mentioned parameters were found to predict the experimental data well (where the hollow dots coincident with the solid dots).

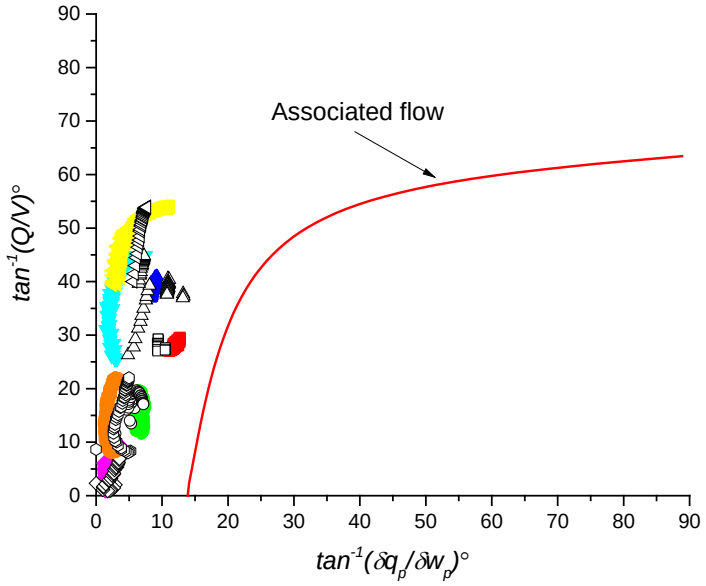

Fig. 18 Associated flow, measured experimental data and predictions from the theoretical non-associated flow

TABLE 2: Force-resultant model parameters

Constant	Dimension	Explanation	Typical values for dense sand of this study	Typical values for loose sand (after [13])	Notes
G	F/L^2	Representative shear modulus			$G = 15.5$ MPa used in the simulation
k_v	-	Elastic stiffness factor (vertical)	2.65	2.65	As defined by Bell (1991)
k_h	-	Elastic stiffness factor (horizontal)	2.3	2.3	
k_m	-	Elastic stiffness factor (moment)	0.46	0.46	
k_c	-	Elastic stiffness factor (horizontal/moment coupling)	-0.14	-0.14	
h_0	-	Dimension of the yield surface (horizontal)	0.174	0.113	Maximum value of H / V_0 on $M = 0$
m_0	-	Dimension of the yield surface (moment)	0.143	0.096	Maximum value of $M / 2RV_0$ on $H = 0$
α	-	Eccentricity if yield surface	-0.042	-0.248	
β_1	-	Curvature factor for the yield surface (low stress)	0.98	0.71	$\beta_1 \le 1.0$, $\beta_2 \le 1.0$
β_2	-	Curvature factor for the yield surface (high stress)	0.99	0.99	
β_3	-	Curvature factor for the plastic potential (low stress)	0.01	0.75	$\beta_3 \le 1.0$, $\beta_4 \le 1.0$
β_4	-	Curvature factor for the plastic potential (high stress)	0.68	0.58	
α_h	-	Curvature factor for the plastic potential	3.3	2.5	
α_m	-	Curvature factor for the plastic potential	6.1	2.5	
c	F	Hardening law parameters	151.85/855.8	278	Fitted from experimental data
k_1	L		0.00074/156.13	0.15	
k_2	F/L		109.73/0.04	0.04	
μ	-	Sliding surface parameters	1	1	Derived analytically
ϖ	-		3	4	Derived analytically

RETROSPECTIVE ANALYSES

The plasticity model was implemented into a FORTRAN programme. For simplicity, the sliding surface was not included in the programme, as more tests are needed before its behaviour is fully understood. Numerical back analyses were performed for a number of representative experiments to evaluate the performance of the modified Model *C* to predict footing behaviour. Fig. 19 compares experiment S_D_VP1 with the program prediction; good agreement was achieved, implying the hardening law and elastic stiffness coefficients are suitable.

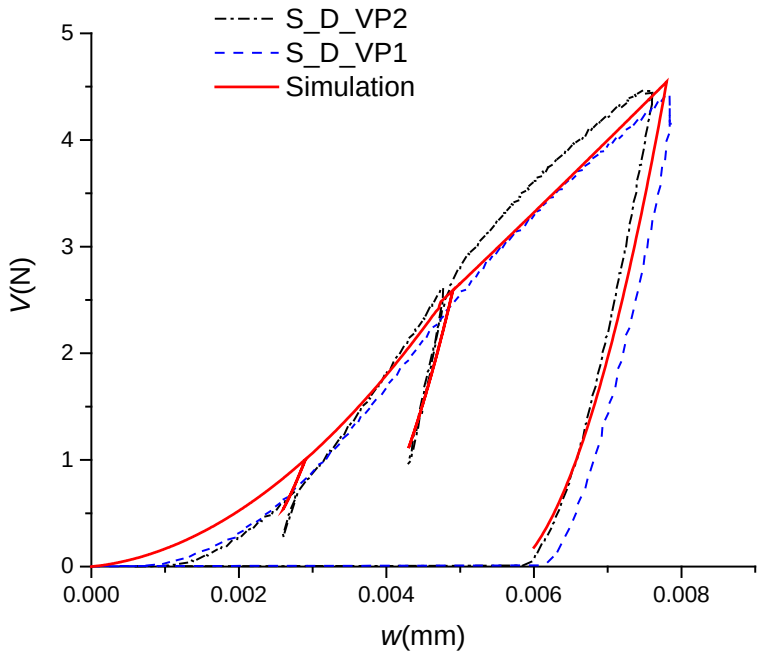

Fig. 19 Associated and non-associated flows and the measured experimental data

Two typical swipe tests S_D_SW1 and S_D_SW3, as previous discussed, were back calculated and presented in Fig. 20 and Fig. 21. As shown in Fig. 20, the program predicts the horizontal swipe tests very well, with only slight overshooting of the prediction of the 'parallel point', where eventually both vertical and horizontal load states stabilised, despite continued horizontal displacement.

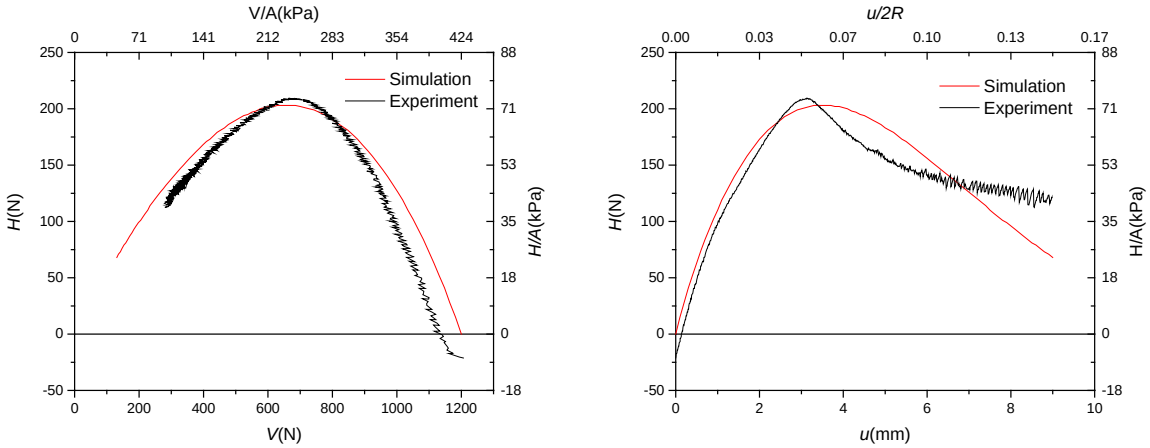

Fig. 20 Comparison between experiment S_D_SW1 and the programme prediction

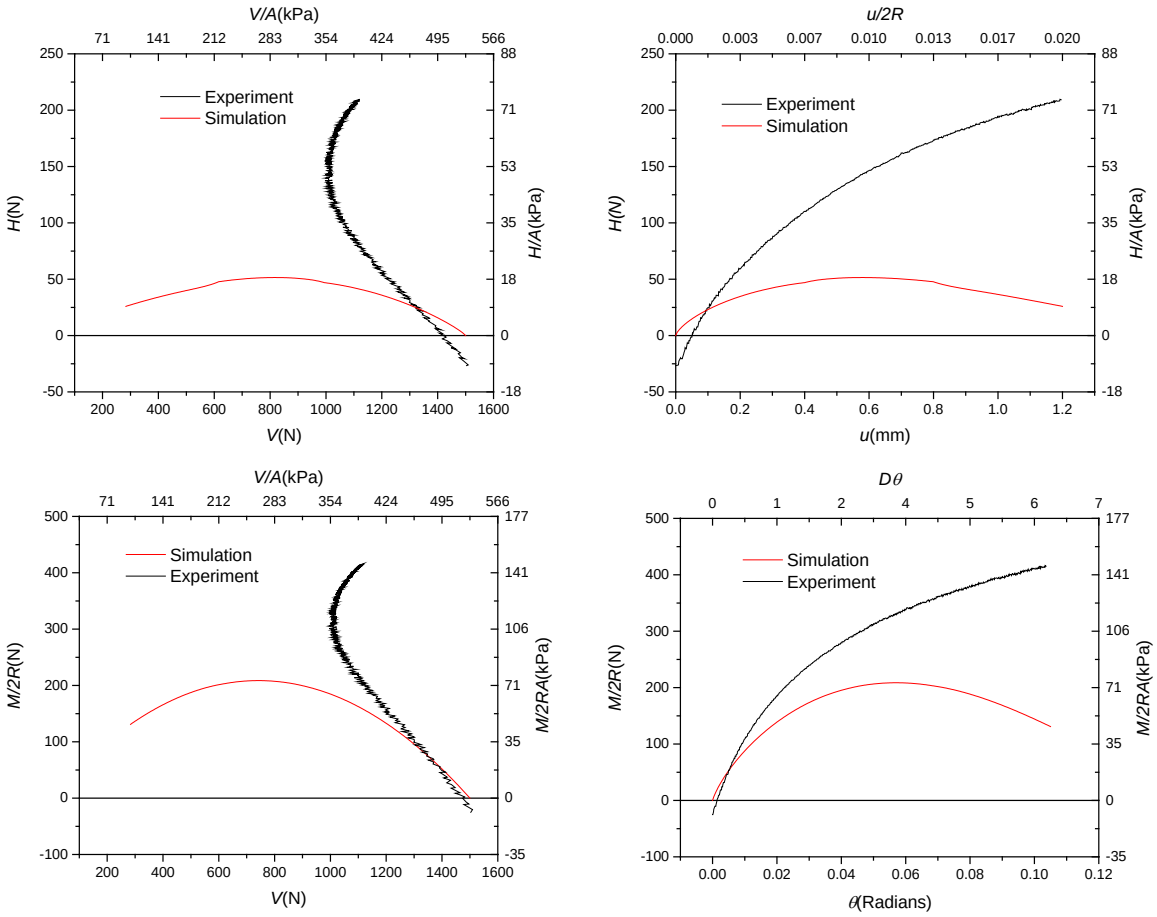

Fig. 21 Comparison between experiment S_D_SW3 and the programme prediction

For swipe test S_D_SW3 with high moment loading, the horizontal load-displacement response predicted by the model is found to follow the experimental data well in the initial stage; however, the experimental and simulated load paths subsequently diverge. This discrepancy is believed to be attributed to two reasons: (i) inability to capture the strong dilatancy behaviours in dense sand under high stress and (ii) the absence of the sliding surface in the programme.

Constant gradients of horizontal to vertical and moment to vertical displacement were used as inputs to simulate the horizontal and moment radial displacements tests. The modified Model C predictions and the corresponding experimental horizontal and moment loads (S_D_RD1,) are shown in Fig. 22.

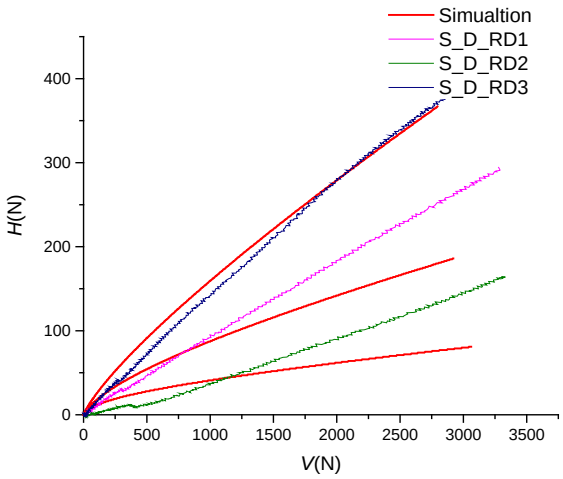

Fig. 22 Comparison between the radial displacement tests and the programme predictions

CONCLUSIONS

This paper presented centrifuge experimental observations of a spudcan model subjected to combined loadings on dense sand under stress levels relevant to offshore conditions. The experimental data were successfully interpreted in terms of the force resultants in the context of strain-hardening plasticity theory, confirming the capability of the approach with respect to the description of the drained response of a spudcan footing under combined loadings. The proposed force resultant model was implemented into a FORTRAN programme capable of being integrated into numerical analysis. Back-analysis of the experimental results using this programme confirms its suitability for use in engineering practice as results are on the conservative side. In addition to the model development, the following key observations of this study are:

a) The yield surface obtained on dense sand in the present study is substantially larger than the results in previous 1-g studies or centrifuge studies of loose sand. Therefore, for spudcans in dense sand the previous model parameters are deemed to be conservative. [23] recommended $h_0 = 0.113$ and $m_0 = 0.08$ for the bearing capacities of spudcan loose sand condition. This paper shows evidence of larger value should be adopted for dense sand conditions. As such an equation has been proposed by [6] in their 1-g tests to quantify these differences. However, caution should be carried out as this method requires the value of V/V_{peak} to be accurately predetermined. It also should be noted that evidence from the current study has slightly lower values of combined bearing capacities.

b) Similar to the test conducted in loose sand, a sliding surface was also observed and identified; the analytical equation used to describe the sliding surface on loose sand was modified accordingly to incorporate the strong dilation behaviour observed in the present study.

c) The recalibrated Model *C* is able to replicate the fundamental behaviours of the spudcan under general loading conditions. Results were shown to be slightly conservative. Formulating a more advanced plasticity model that incorporates the sliding surface should be developed in the future.

ACKNOWLEDGEMENTS

The first author acknowledges the support of the Australian Postgraduate Awards. The second author acknowledges the support of the ARC through his Australian Laureate Fellowship (FL130100059) and also acknowledges the Lloyd's Register Foundation (LRF). LRF a UK registered charity and sole shareholder of Lloyd's Register Group Ltd, invests in science, engineering and technology for public benefit, worldwide. This support is gratefully acknowledged. The authors thank the following colleagues and technical staff at the Centre for Offshore Foundation Systems at the University of Western Australia, who provided invaluable support during the instrumentation of the centrifuge test: Mr. Shane De Catania, Mr. Bart Thompson, Dr. Youhu Zhang, and Dr. Conleth O'Loughlin.

REFERENCES

[1] Bell, R. 1991. The analysis of offshore foundations subject to combined loading. MSc thesis, University of Oxford.

[2] Bienen, B., Byrne, B. W., Houlsby, G. T. & Cassidy, M. J.- Investigating six-degree-of-freedom loading of shallow foundations on sand. Géotechnique1.2006:56(6):367-380.

[3] Bienen, B., Gaudin, C. & Cassidy, M. J.- Centrifuge tests of shallow footing behaviour on sand under combined vertical-torsional loading. International Journal of Physical Modelling in Geotechnics1.2007:7(2):1-21.

[4] Bolton, M. D.- The strength and dilatancy of sands. Geotechnique1.1986:36(1):65-78.

[5] Butterfield, R., Houlsby, G. T. & Gottardi, G.- Standardized sign conventions and notation for generally loaded foundations. Géotechnique1.1997:47(5):1051-1054.

[6] Byrne, B. W. & Houlsby, G. T.-Drained behaviour of suction caisson foundations on very dense sand. Offshore Technology Conference, Houston, TX, 1999.p 3-6.

[7] Byrne, B. W. & Houlsby, G. T.- Observations of footing behaviour on loose carbonate sands. Géotechnique1.2001:51(5):463-466.

[8] Cassidy, M. J.- Experimental observations of the combined loading behaviour of circular footings on loose silica sand. Geotechnique1.2007:57(4):397-401.

[9] Cassidy, M. J., Byrne, B. W. & Houlsby, G. T.- Modelling the behaviour of circular footings under combined loading on loose carbonate sand. Géotechnique1.2002:52(10):705-712.

[10] Cassidy, M. J. & Houlsby, G. T.- Vertical bearing capacity factors for conical footings on sand. Géotechnique1.2002:52(9):687-692.

[11] Cassidy, M. J., Houlsby, G. T., Hoyle, M. & Marcom, M. R.-Determining appropriate stiffness levels for spudcan foundations using jack-up case records. 21st International Conference on Offshore Mechanics and Arctic Engineering, 2002.p 307-318.

[12] Cheng, N. & Cassidy, M. J. (2015). Combined Loading Capacity of Spudcan Footings on Loose Sand. *International Journal of Physical Modelling in Geotechnics*,accepted

[13] Cheng, N. & Cassidy, M. J. (2015). Development of a force resultant plasticity model for spudcans on loose sand. *Journal of Offshore Mechanics and Arctic Engineering*,submitted

[14] Cheng, N., Gaudin, C., Cassidy, M. J. & Bienen, B.-Centrifuge study of the combined bearing capacity of a hybrid foundation system. 8th International Conference on Physical Modelling in Geotechnics, Perth, 2014.p 487-492.
[15] Cocjin, M. & Kusakabe, O.- Centrifuge observations on combined loading of a strip footing on dense sand. Géotechnique1.2012:63(5):427-433.
[16] Doherty, J. P. & Deeks, A. J.- Elastic response of circular footings embedded in a non-homogeneous half-space. Géotechnique1.2003:53(8):703-714.
[17] Gottardi, G. & Butterfield, R.- On the bearing capacity of surface footings on sand under general planar loads. Soils and Foundations1.1993:33(3):68-79.
[18] Gottardi, G. & Butterfield, R.- The displacement of a model rigid surface footing on dense sand under general planar loading. Soils and Foundations1.1995:35(3):71-82.
[19] Gottardi, G., Houlsby, G. T. & Butterfield, R.- Plastic response of circular footings on sand under general planar loading. Géotechnique1.1999:49(4):453-469.
[20] Govoni, L., Gourvenec, S. & Gottardi, G.- Centrifuge modelling of circular shallow foundations on sand. International Journal of Physical Modelling in Geotechnics1.2010:10(2):35-46.
[21] Govoni, L., Gourvenec, S. & Gottardi, G.- A centrifuge study on the effect of embedment on the drained response of shallow foundations under combined loading. Géotechnique1.2011:61(12):1055-1068.
[22] Houlsby, G. T. & Cassidy, M. J.- A plasticity model for the behaviour of footings on sand under combined loading. Géotechnique1.2002:52(2):117-129.
[23] ISO. (2012). Petroleum and natural gas industries-Site specific assessment of mobile offshore units - Part 1:Jack-ups, 19905-1. International Organization for Standardization.
[24] Martin, C. M. & Houlsby, G. T.- Combined loading of spudcan foundations on clay: laboratory tests. Géotechnique1.2000:50(4):325-338.
[25] National Instrument Corporation 2003. LabVIEW User Manual. National Instrument Corporation.
[26] Ngo-Tran, C. 1996. The analysis of offshore foundations subjected to combined loading. Dphil thesis, University of Oxford.
[27] Nova, R. & Montrasio, L.- Settlements of shallow foundations on sand. Géotechnique1.1991:41(2):243-256.
[28] Schneider, J. A. & Lehane, B. M.-Effects of width for square centrifuge displacement piles in sand. Proceedings of the 6th International Conference on Physical Modelling in Geotechnics, Hong Kong, 867-873.
[29] Stewart, D., Boyle, R. & Randolph, M. F.-Experience with a new drum centrifuge. International conference centrifuge, Tokyo, 1998.p 35-40.
[30] Vlahos, G., Cassidy, M. J. & Martin, C. M.- Numerical simulation of pushover tests on a model jack-up platform on clay. Geotechnique1.2011:61(11):947-960.
[31] White, D. J., Teh, K. L., Leung, C. F. & Chow, Y. K.- A comparison of the bearing capacity of flat and conical circular foundations on sand. Géotechnique1.2008:58(10):781-792.
[32] Yun, G. J. & Bransby, M. F.-Centrifuge modeling of the horizontal capacity of skirted foundations on drained loose sand. Proc. International Conference on Foundations, Dundee, Scotland, 1-10.
[33] Zhang, Y., Bienen, B. & Cassidy, M. J.- Development of a combined VHM loading apparatus for a geotechnical drum centrifuge. International Journal of Physical Modelling in Geotechnics1.2013:13(1):13-30.